Testing for Welding, Joining or Additive Manufacturing Applications

Sinan Aydin*

TIG-weldability of AISI 430 and DUROSTAT 500 grade

Abstract: In this study, 10 mm thick DUROSTAT 500 and AISI 430 grades were joined by double sided keyhole tungsten inert gas (K-TIG) welding method without using filler material. The characterization of the microstructure of the weld zone was investigated by optical analysis methods and the mechanical properties of the welded parts were examined by mechanical tests. The fracture surface structure of the parts that were broken as a result of the tests were examined. No deterioration was observed in the welded samples. It was determined that the weld penetration increased as a result of the increase in the amount of heat entering the weld zone with the increasing welding current.

Keywords: AISI 430; DUROSTAT 500; K-TIG; microstructure; weldability.

1 Introduction

Tungsten inert gas welding (TIG) is an arc welding method that is widely used in industry. Due to the increasing demand for the welding of medium and thick section parts in the industry; TIG welding types such as multi-electrode TIG, keyhole TIG (K-TIG), activated TIG and pulsed TIG have emerged [1]. Due to the low arc current used in TIG welding, the productivity is low and the penetration ability is very poor. A method, called keyhole K-TIG, has emerged where higher welding current and arc pressure are used to increase the penetration ability [2].

K-TIG has superiority over traditional TIG welding in terms of penetration ability, energy density and welding productivity [3]. K-TIG is highly advantageous over the traditional TIG method due to the fact that it is possible to weld with full penetration in a single pass up to a thickness of

16 mm, in addition to the savings obtained during the welding process without the use of filler material and edge chamfering [4].

Zhenyu et al. [5] provided full penetration in a single pass without the need for additional material and edge arrangement with the K-TIG method. They stated that it could be a way of cheap and highly efficient welding of medium thickness steels without deteriorating the mechanical properties of the welded materials.

Stainless steels can be grouped as martensitic, duplex and austenitic-ferritic stainless steels (FSS) according to their crystal structures. AISI 430, a type of FSS, is used in many areas today, but its resistance to corrosion is weak. FSS has very low carbon content. Ductility, low strength etc. has features. Chromium in its content inhibits resistance against corrosion [6].

FSS are more resistant to corrosion cracking and stress than austenitic stainless steels, making them a more economical option than austenitic stainless steels for corrosion-related processes. FSS have low thermal expansion and high thermal conductivity, making them an ideal material for heat exchangers and coatings [7].

Ramkumar et al. [8] investigated the mechanical properties, microstructure and weldability of AISI 430 steel combined with TIG welding. They determined that there are widmanstätten ferrite, ferrite and low carbon content martensite heaps in the source transition zone of the samples. They observed that in the weld fusion zone, the hardness was higher than the base metal, there were more martensite grains at the heat affected zone grain boundaries of all test specimens and grain coarsening.

Swedish steelmaker SSAB AB produces Hardox steel, which is called wear-resistant martensitic boron steel. In addition, other manufacturers; for example, Grobblech GmbH (Durostat), Dillinger Hütte GTS (Dillidur steels), Thyssen Krupp Steel Europe AG (TBL and XAR steels), AcelorMittal (Usibor), JFE EVERHARD Corporation (JFE-EH), SUMITOMO Metal (Sumihard), and TITUS Steel (Endura), TATA Steel Group (Abrazo) manufactures modern boron steels with high wear resistance [9, 10].

DUROSTAT 500 steels are used extensively in the manufacture of loader buckets, wagon bodies, conveyors

*Corresponding author: Sinan Aydin, Department of Mechatronics Engineering, Faculty of Technology, Sivas Cumhuriyet University, Sivas, 58140, Türkiye, E-mail: sinancan@cumhuriyet.edu.tr. https://orcid.org/0000-0003-2285-0906

and excavator components, due to their high resistance to wear [11].

Teker et al. [12] used three different welding currents with double sided keyhole TIG welding method and welded 10 mm thick steel plates in the butt position without pretreatment. They observed that the amount of penetration increased with the increase of the welding current used in the symmetric sand-watch shaped weld samples. In addition, in another study, they combined HARDOX 450 and AISI 430 steel with double sided TIG welding. They investigated the microstructure of the weld zone and the properties of the welded joint HAZ [13].

In this study, AISI 430 and DUROSTAT 500 steels were joined by double sided K-TIG arc welding method, and the microstructure of the welding zone and the mechanical properties of the formed joint were investigated.

2 Experimental approach

DUROSTAT 500 and AISI 430 steel plates measuring 10 × 100 × 130 mm were used in the welded joints. In Table 1, the chemical content of DUROSTAT 500 and AISI 430 steels, in Table 2, the mechanical properties of the steels, in Table 3 the welding parameters and in Table 4, the devices used are given.

Steel plates prepared before welding are given in Figure 1.

After the test samples are combined with the K-TIG welding method; microstructural analysis samples, tensile test samples (conforming to EN-ISO 6892-1) and notch impact test samples (conforming to EN-ISO 148-3) were taken in the dimensions given in Figure 2. In Figure 3, the extracted test samples are given.

The samples were sanded with 80–1200 grit SiC papers in a 200 mm diameter double disc device and polished using paste. DUROSTAT 500 was etched with a 2% HNO_3 + 98% alcohol. AISI 430 was etched with DC 12 V for 3 s with 50% HNO_3 + 50% alcohol [12]. Microstructural analysis of welded joints was performed with OM and SEM. Tensile and notch impact tests were performed on the test samples. Elemental compositions of the welded joint were investigated by EDS.

Table 2: Mechanical properties of steels.

Material	Hardness (HB)	Yield strength (MPa)	Tensile strength (MPa)	Fracture elongation (%)
AISI 430	183	345	517	22
DUROSTAT 500	500	1200	1550	8

3 Results and discussion

The cross-sectional view of the welded joints of 3 samples is given in Figure 4. There was no distortion in the welded samples, and quality weld seams were obtained without any deviations and depressions. When the microstructures of the samples were examined, no deterioration was detected due to the heat generated in the weld area.

The largest gap between the parts joined in double sided welding occurred in Sample 1. As a result of the increase in the heat density entering the weld area with the increasing welding current, the penetration of the weld was increased, full contact was achieved in Sample 3 without leaving any gaps and a sand-watch shape was formed.

During the welding process, the welding arc is directed towards the ferromagnetic material side [14]. The way to create a good weld profile geometry is to select the appropriate welding current. Due to the high cooling rate during the solidification of the weld metal, the temperature variation between the edge and the weld center is large. Therefore, the crystal structure grows in the direction of the region with the maximum temperature.

The surface tension gradient expresses the convection movements on the surface of the weld zone. Since the gradient is negative in TIG welding, the convection movements are outward, so the penetration depth is less. With the addition of active flux, the convection currents reverse and change the gradient sign, so the convection movements take place inward centriply increasing the depth of penetration.

In the K-TIG welding method, the surface tension in the weld center is higher than the edges, due to the change of the temperature coefficient of the surface tension on the

Table 1: Chemical content of steels.

Material	Chemical content (wt%)									
	Fe	C	Si	Mn	Cr	Ni	S	Mo	B	Ti
AISI 430	Bal.	0.048	0.44	0.61	16.02	0.22	0.002	0.016	–	–
DUROSTAT 500	Bal.	0.30	0.60	2.1	1	–	0.01	0.5	0.05	0.05

Table 3: TIG welding parameters.

Sample	Electric current (A)	Electrical voltage (V)	Shielding gas flow rate (l min^{-1})	Welding speed (m min^{-1})	Nozzle diameter (mm)	Electrode diameter (mm)
1	230	100	15	0.01	8	2.5
2	260	105	15	0.01	8	2.5
3	290	110	15	0.01	8	2.5

Table 4: Used devices.

Process	Device brand/model
TIG welding	Ge-Ka-Mak Power TIG
Surface preparation (Sanding and polishing)	AOB/POL BULUPOL
Scanning electron microscope (SEM) analysis	Tescan Mira3
Energy dispersive spectroscopy (EDS) analysis	Tescan Mira3
Optical microscope (OM) analysis	Nikon Eclipse LV150
Microhardness analysis	Shimadzu HMV-G
Tensile test	Instron 3367 (30 KN)
Notch impact test	Instron Dynatup 9250 (300 J)
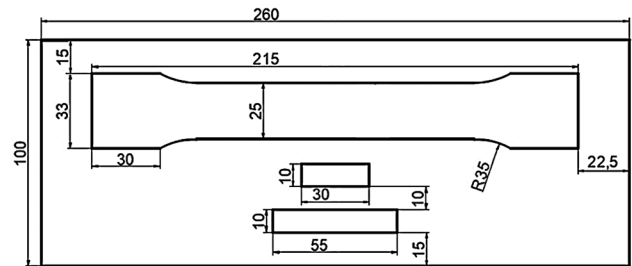
Figure 2: Test samples dimensions.

weld pool to be positive, thus deep penetration is obtained [15].

Optical microstructure of Sample 3 is given in Figure 5 and SEM image is given in Figure 6. It has been determined that while the welding transition zone is separated sharply on the AISI 430 side, the DUROSTAT 500 side is spread over a wider area. Grain boundary carbides and grain inner carbides were detected on the AISI 430 side, Widmanstätten ferrite, acicular ferrite and martensite were detected on the DUROSTAT 500 side.

In Figure 7, XRD analysis result graph of Sample 3 is given. Fe, Cr_7C_3, Cr_3Ni_3, $Cr_{1.36}Fe_{0.52}$, $Cr_{23}C_6$ and Fe_3Ni_2 phases and compounds were observed.
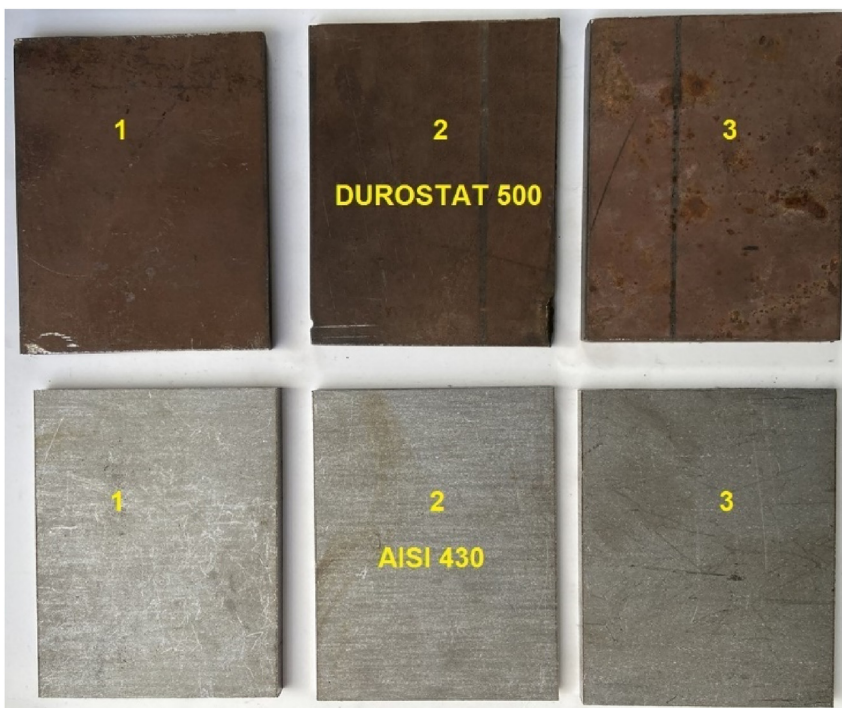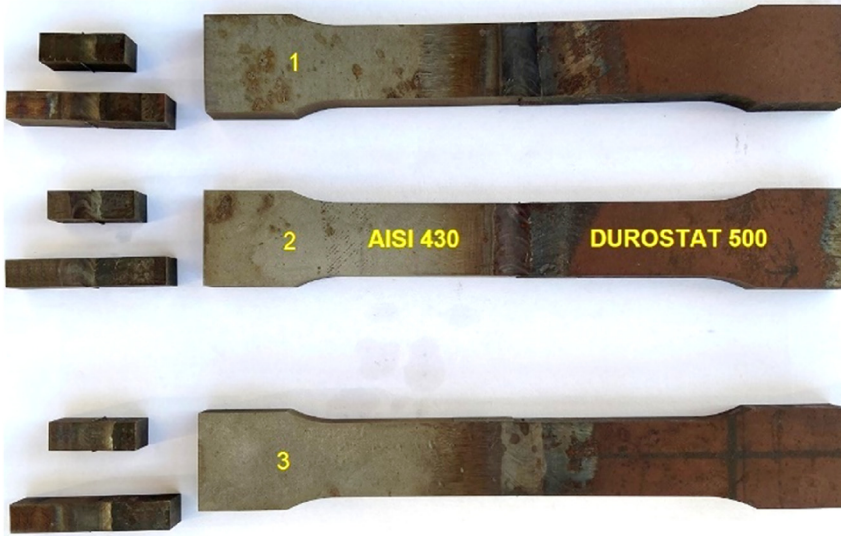

Figure 1: Steel plates prepared before welding.
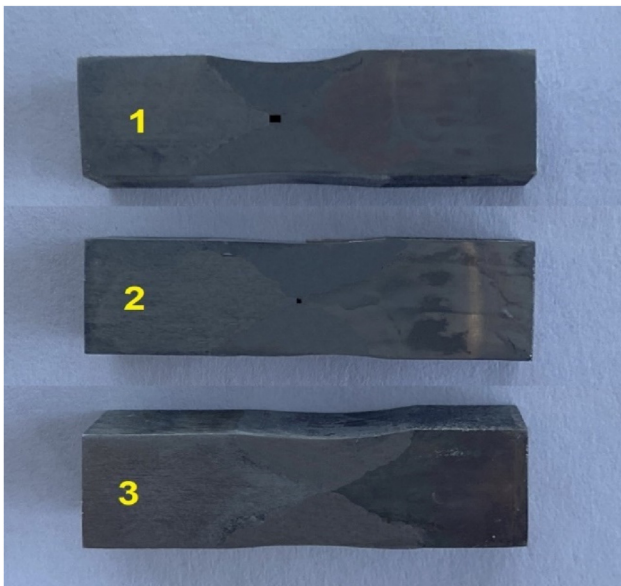
Figure 3: Test samples.

Figure 4: The cross-sectional view of the welded joints.

Figure 5: Optical microstructure of sample 3.

EDS analysis points on weld metal and HAZ of Sample 3 are given in Figure 8 and EDS values are given in Table 5. Fe, Cr, C, Mn, Si and Ni elements were detected in these zones. In the AISI 430 zone; while there was no significant change in the amount of C, a significant decrease in the amount of Cr and increase in the amount of Fe were observed. In the DUROSTAT 500 zone; there was an increase in the amount of C, a decrease in the amount of Cr and Fe.

The microhardness measurements of the samples are given in Figure 9. The microhardness results of the non-welded zone were lower than the welded zone. The batten type m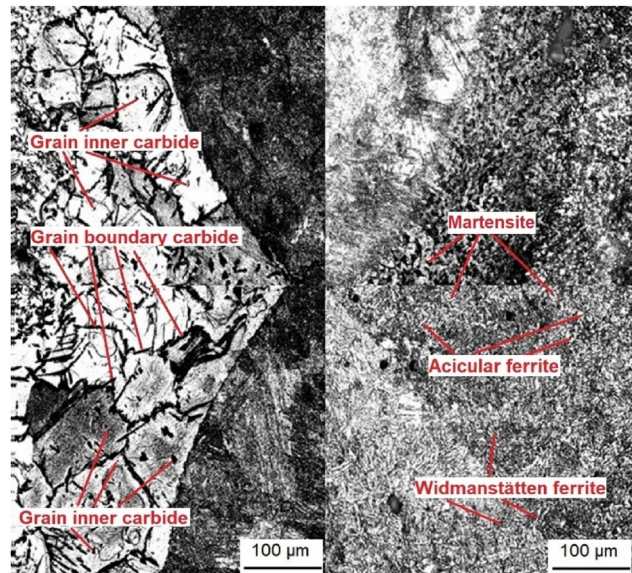artensite structure formed due to the rapid cooling during the solidification of the weld metal provided an increase in hardness. Due to the slow cooling in the fusion zone, the transition time of Cr and Fe from FSS to the weld metal was prolonged, so more atoms crossed the fusion line, causing the plastic deformation resistance of FSS in the HAZ to worsen. Due to the homogeneity of the phase distribution throughout the weld penetration region, the hardness distribution was homogeneous. The highest hardness value was measured at 477 HV in the upper region weld center of Sample 3. The hardness increased from 210 HV to 459 HV on the sample upper region AISI 430 side and increased from 182 HV to 464 HV on the DURO-STAT 500 side. Hardness was measured at 465 HV in the
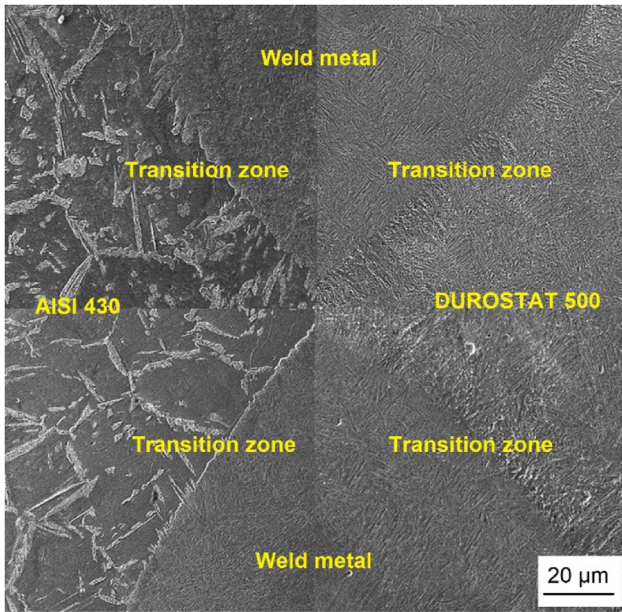
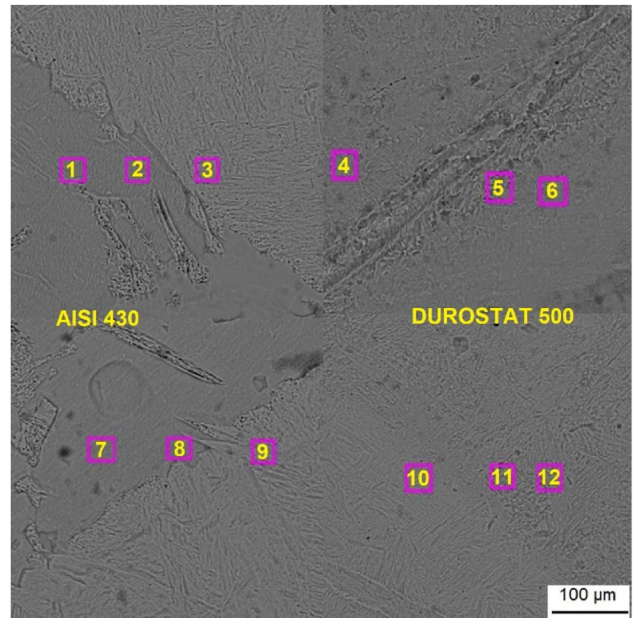**Figure 6:** SEM image of sample 3.

Figure 8: EDS analysis results of sample 3.

lower region weld center of Sample 3. The hardness increased from 199 HV to 440 HV on the sample subzone AISI 430 side and increased from 188 HV to 462 HV on the DUROSTAT 500 side.

The images of the samples subjected to the tensile test are given in Figure 10, and the test results graph is given in Figure 11. Since the resistance of the fine-grained structures in HAZ to deformation is higher than the base metal, rupture has occurred in the base metal parts with larger grain structure. Tensile strengths increased due to increased penetration due to increased current intensity. The highest tensile strength was measured as 497 MPa in Sample 3, which provided the best weld penetration.

The fracture surface SEM image of Sample 3 after the test is given in Figure 12. Brittle fracture occurred in the sample due to homogeneous cavities and voids on the AISI 430 and DUROSTAT 500 sides of the sample.

The highest value was obtained in Sample 3 with 112 J. Due to the higher hardness values in the weld area than the other samples, the notch impact strength of Sample 3 was higher than the other samples. Since AISI 430 has a structure that is approximately 3 times softer than DUROSTAT 500, the fractures in the samples occurred in the region closer to the AISI 430 side.

Due to the increase in the volume of acicular ferrite in the weld area, the energy absorbed in the notch impact test
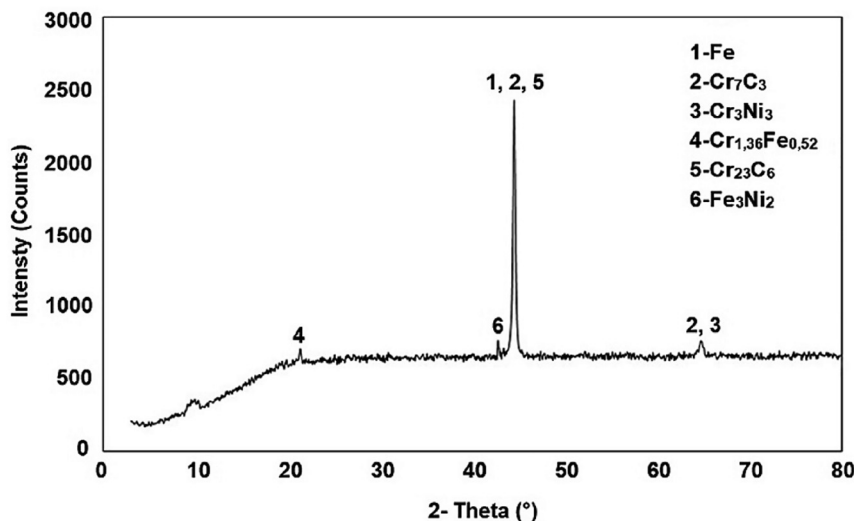

Figure 7: XRD analysis result graph of sample 3.

Table 5: EDS values of Sample 3.

Point	Elements (wt%)					
	Fe	Cr	C	Mn	Si	Ni
1	77.92	16.47	4.47	0.61	0.37	0.16
2	79.48	15.96	3.63	0.45	0.32	0.16
3	82.13	12.26	4.43	0.55	0.41	0.22
4	90.05	0.64	7.88	0.69	0.32	0.42
5	88.61	0.63	9.41	0.66	0.32	0.37
6	87.79	0.62	10.10	0.74	0.32	0.43
7	78.83	15.96	4.16	0.54	0.39	0.12
8	80.85	14.92	3.07	0.63	0.35	0.18
9	83.64	11.28	3.84	0.64	0.36	0.24
10	89.25	0.65	8.86	0.59	0.36	0.29
11	89.00	0.63	8.96	0.64	0.37	0.40
12	88.87	0.61	9.25	0.60	0.31	0.36

increases. Acicular ferrite has a higher toughness value between Widmanstätten ferrite and pearlitic–ferritic phase structures. Due to the interlocking structure and fine grain size of acicular ferrite, it provides the highest level of resistance against crack propagation [16]. These structures on the DURO-STAT 500 side have increased the resistance against impact.

In K-TIG welding; welding is carried out without filler metals by melting and solidification of adjacent base metals. Therefore, the weld microstructure is only affected by the weld thermal cycle, without a change in the chemical content of the weld metal. The small grain sizes formed after welding cause an increase in the number of grains per unit volume, and the probability of stress cracking due to stress accumulation decreases so much that the notch impact toughness also increases (Figures 13 and 14).
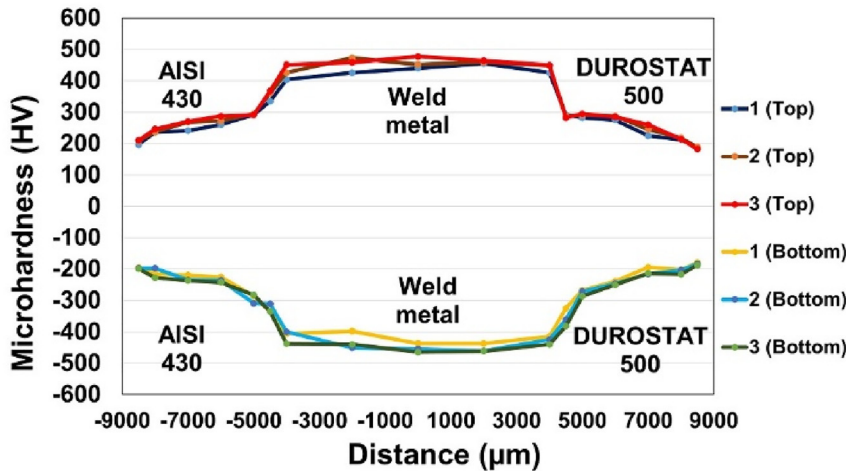

Figure 9: Microhardness results of samples.

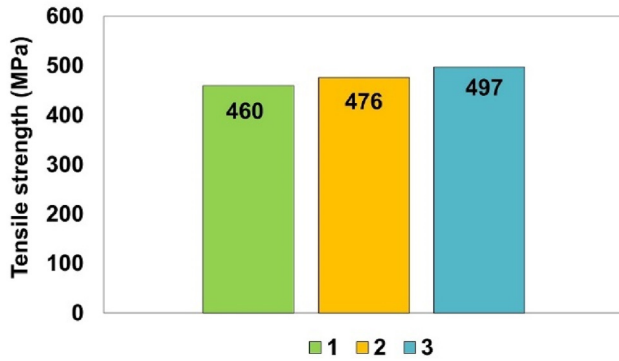**Figure 10:** Image of samples after tensile test.

Figure 11: Tensile test results.

The weld samples showed a more brittle condition due to the formation of lath martensite phases, which increased the material strength [17].

4 Conclusions

Phase and chemical structure analyzes of the welded joints formed with DUROSTAT 500 and AISI 430 steels were made. The following results were obtained.

(1) AISI 430 and DUROSTAT 500 steels were joined in a single pass without the use of additional wire and without opening the weld.

(2) During welding, ideal sand-watch form and full penetration were obtained by increasing the current intensity.

(3) Grain boundary carbides and grain inner carbides were detected on the AISI 430 side, acicular ferrite, martensite and Widmanstätten ferrite were detected on the DUROSTAT 500 side.

(4) Fe, Cr_7C_3, Cr_3Ni_3, $Cr_{1.36}Fe_{0.52}$, $Cr_{23}C_6$ and Fe_3Ni_2 compounds were observed in the weld metal.
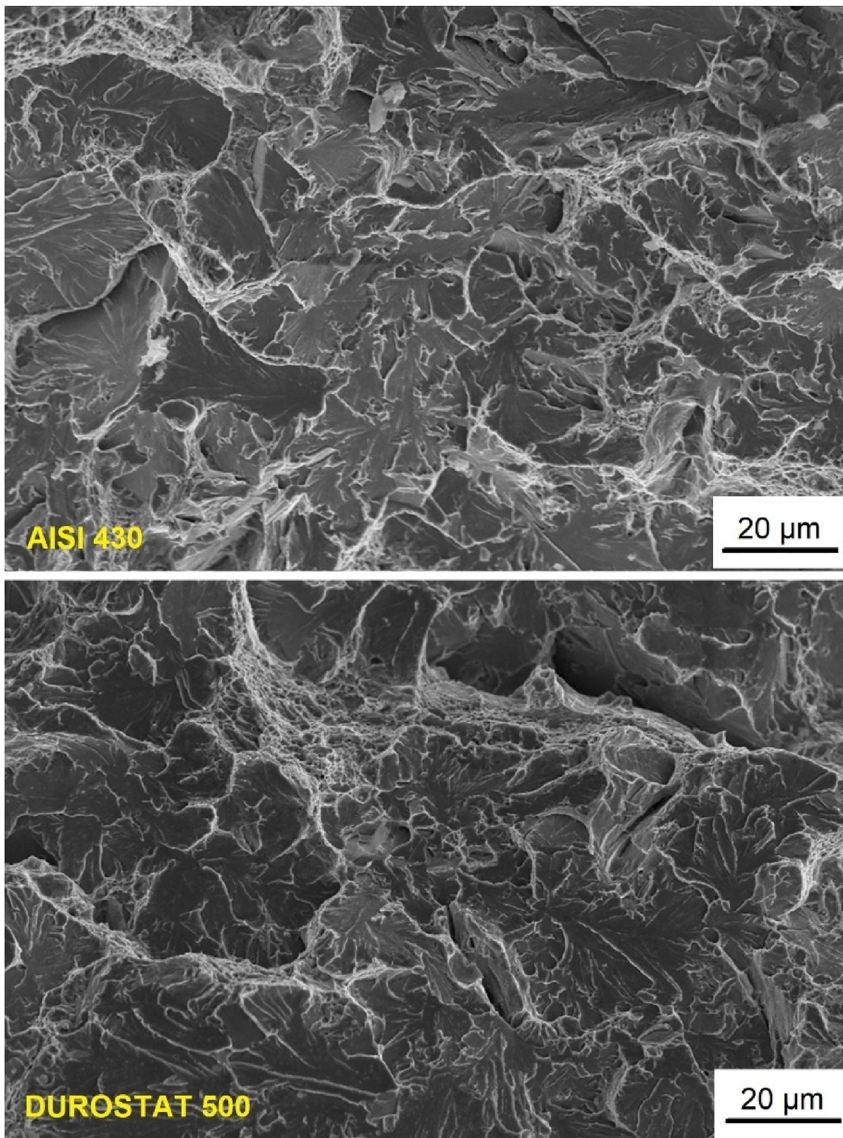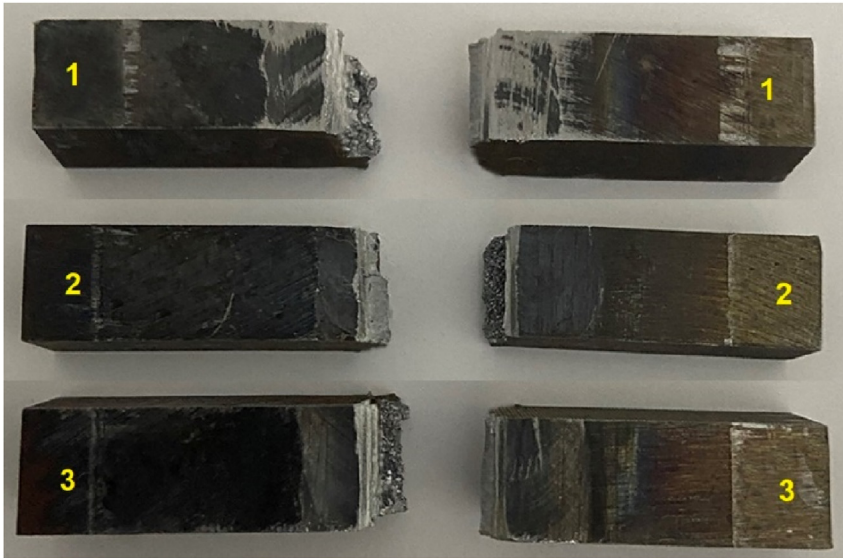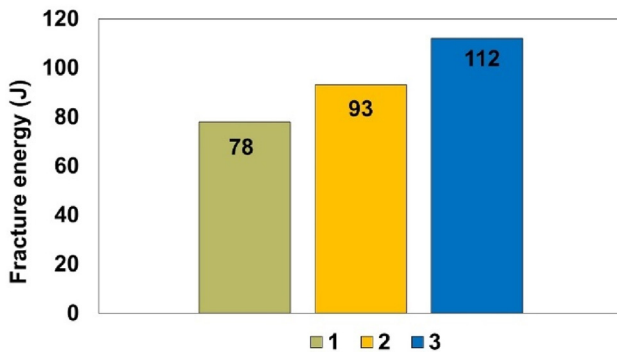

Figure 12: The fracture surface SEM image of sample 3.

Figure 13: Fracture photos of samples after notch impact test.

Figure 14: Notch impact test results.

(5) Tensile strength and notch impact strength increased linearly with increasing current intensity. The maximum tensile strength value was 497 MPa and the notch impact test fracture energy maximum value was 112 J in Sample 3.

(6) As a result of mechanical tests, brittle fracture occurred in the samples.

References

[1] K. Kumar, C. S. Kumar, M. Masanta, and S. Pradhan, "A review on TIG welding technology variants and its effect on weld geometry," *Mater. Today: Proc.*, vol. 50, pp. 999–1004, 2022, https://doi.org/10.1016/j.matpr.2021.07.308.

[2] X. Chunyang, P. Zengxi, F. Zhenyu, Z. Shiyu, and L. Huijun, "Vision based defects detection for Keyhole TIG welding using deep learning with visual explanation," *J. Manuf. Process.*, vol. 56, pp. 845–855, 2020, https://doi.org/10.1016/j.jmapro.2020.05.033.

[3] L. Z. Ming, F. Y. Xiao, C. S. Lin, et al., "Stable keyhole welding process with K-TIG," *J. Mater. Process. Technol.*, vol. 238, pp. 65–72, 2016, https://doi.org/10.1016/j.jmatprotec.2016.07.005.

[4] C. Shuwan, S. Yonghua, Z. Tao, and L. Weicong, "Microstructure, texture, and mechanical properties of Ti-6Al-4V joints by KTIG welding," *J. Manuf. Process.*, vol. 37, pp. 418–424, 2019, https://doi.org/10.1016/j.jmapro.2018.12.022.

[5] F. Zhenyu, P. Zengxi, C. Dominic, et al., "Investigation into the viability of K-TIG for joining armour grade quenched and tempered steel," *J. Manuf. Process.*, vol. 32, pp. 482–493, 2018, https://doi.org/10.1016/j.jmapro.2018.03.014.

[6] M. Vamshi, S. K. Singh, N. Sateesh, D. S. Nagaraju, and R. Subbiah, "A review on influence of carburizing on ferritic stainless steel," *Mater. Today: Proc.*, vol. 26, pp. 937–943, 2020, https://doi.org/10.1016/j.matpr.2020.01.151.

[7] G. M. Reddy, T. Mohandas, A. S. Rao, and V. V. Satyanarayana, "Influence of welding processes on microstructure and mechanical properties of dissimilar austenitic-ferritic stainless steel welds," *Mater. Manuf. Processes*, vol. 20, pp. 147–173, 2005, https://doi.org/10.1081/AMP-200041844.

[8] K. D. Ramkumar, A. Chandrasekhar, A. K. Singh, et al., "Comparative studies on the weldability, microstructure and tensile properties of autogeneous TIG welded AISI 430 ferritic stainless steel with and without flux," *J. Manuf. Process.*, vol. 20, pp. 54–69, 2015, https://doi.org/10.1016/j.jmapro.2015.09.008.

[9] B. Bialobrzeska, R.. Jasinski, Ł. Konat, and Ł. Szczepanski, "Analysis of the properties of Hardox extreme steel and possibilities of its applications in machinery," *Metals*, vol. 11, pp. 162, 2021, https://doi.org/10.3390/met11010162.

[10] B. Bialobrzeska and P. Kostencki, "Abrasive wear characteristics of selected low-alloy boron steels as measured in both field experiments and laboratory tests," *Wear*, vols. 328–329, pp. 149–159, 2015, https://doi.org/10.1016/j.wear.2015.02.003.

[11] T. Teker and A. Günes, "Microstructure and mechanical properties of AISI 304/DUROSTAT 500 steel double sided TIG welds," *Mater. Test.*, vol. 64, no. 8, pp. 1162–1171, 2022, https://doi.org/10.1515/mt-2022-0033.

[12] T. Teker, E. M. Karakurt, and F. Demir, "Mechanical property effects of symmetrical hour glass shapes formed during double sided TIG keyhole arc welding of AISI 1040 joints," *Mater. Test.*, vol. 59, no. 6, pp. 524–529, 2017, https://doi.org/10.3139/120.111041.

[13] T. Teker and D. Gencdogan, "Heat affected zone and weld metal analysis of HARDOX 450 and ferritic stainless steel double sided TIG-joints," *Mater. Test.*, vol. 63, no. 10, pp. 923–928, 2021, https://doi.org/10.1515/mt-2021-0022.

[14] R. P. Reis, D. Souza, and A. Scotti, "Models to describe plasma jet, arc trajectory and arc blow formation in arc welding," *Weld. World*, vol. 55, pp. 24–32, 2011, https://doi.org/10.1007/BF03321283.

[15] R. S. Vidyarthy, D. K. Dwivedi, and M. Vasudevan, "Influence of M-TIG and A-TIG welding process on microstructure and mechanical behavior of 409 ferritic stainless steel," *J. Mater. Sci. Eng. Perform.*, vol. 26, pp. 1391–1403, 2017, https://doi.org/10.1007/s11665-017-2538-5.

[16] S. Kou, *Welding Metallurgy*, 3rd ed. New York, USA, John Wiley & Sons Inc, 2003.

[17] K. Hemalatha, C. James, L. Natrayan, and V. Swamynadh, "Analysis of RCC T-beam and prestressed concrete box girder bridges super structure under different span conditions," *Mater. Today: Proc.*, vol. 37, pp. 1507–1516, 2021, https://doi.org/10.1016/j.matpr.2020.07.119.

The author of this contribution

Sinan Aydin
Dr. Sinan Aydin, born in 1975, works in the University of Sivas Cumhuriyet, Faculty of Technology, Department of Mechatronic Engineering, Sivas, Turkey. He graduated in Mechanical Engineering at Cumhuriyet University, Sivas, Turkey, in 1997. He received his MSc degree at Cumhuriyet University, Sivas, Turkey in 2001 and PhD degree at Firat University, Elazig, Turkey, in 2012. He studied solid state welding methods, nano particles and adhesive technologies.